The surface composition of Jupiter Trojans: Visible and near-infrared survey of dynamical families

ARTICLE *in* ICARUS · AUGUST 2006

Impact Factor: 3.04 · DOI: 10.1016/j.icarus.2006.02.012 · Source: OAI

9 AUTHORS, INCLUDING:

E. Dotto
National Institute of Astrophysics
265 PUBLICATIONS **2,330** CITATIONS
SEE PROFILE

Javier Licandro
Instituto de Astrofísica de Canarias
294 PUBLICATIONS **2,655** CITATIONS
SEE PROFILE

Olivier Hainaut
European Southern Observatory
334 PUBLICATIONS **3,936** CITATIONS
SEE PROFILE

F. Marzari
University of Padova
277 PUBLICATIONS **3,273** CITATIONS
SEE PROFILE

Available online at www.sciencedirect.com
SCIENCE DIRECT
Icarus 183 (2006) 420–434
ICARUS
www.elsevier.com/locate/icarus

The surface composition of Jupiter Trojans: Visible and near-infrared survey of dynamical families ☆

E. Dotto [a,*], S. Fornasier [b], M.A. Barucci [c], J. Licandro [d,e], H. Boehnhardt [f], O. Hainaut [g], F. Marzari [h], C. de Bergh [c], F. De Luise [a]

[a] *INAF, Osservatorio Astronomico di Roma, Via Frascati 33, I-00040 Monteporzio Catone (Roma), Italy*
[b] *Department of Astronomy, University of Padova, Vicolo dell'Osservatorio 2, I-35122 Padova, Italy*
[c] *LESIA, Observatoire de Paris-Meudon, 5 Place Jules Janssen, 92195 Meudon, France*
[d] *Isaac Newton Group of Telescopes, P.O. Box 321, E-38700 Santa Cruz de la Palma, Tenerife, Spain*
[e] *Instituto de Astrofisica de Canarias, c/Via Lactea s/n, E-38200 La Laguna, Tenerife, Spain*
[f] *Max Planck Institute for Solar System Research, Max-Planck-Strasse 2, D-37191 Katlenburg-Lindau, Germany*
[g] *European Southern Observatory, Casilla 19001, Santiago, Chile*
[h] *Department of Physics, University of Padova, Via Marzolo 8, I-35131 Padova, Italy*

Received 27 June 2005; revised 14 February 2006

Available online 24 April 2006

Abstract

Asteroid dynamical families are supposed to be formed from the collisional disruption of parent bodies. As a consequence, the investigation of the surface properties of small and large family members may give some hints on the nature of the dynamical group, the internal composition of the parent body, and the role played by space weathering processes in modifying the spectral behavior of the members' surfaces. In this work we present visible–near-infrared observations of 24 Jupiter Trojans belonging to seven dynamical families of both the L4 and L5 swarms. The most important characteristics we found is the uniformity of the Trojans population. All the investigated Trojans have featureless spectra and a spectral behavior typical of the primitive P and D taxonomic classes. In particular, no signatures of water ice have been found on the spectra of these primordial bodies. From our investigation, the L4 and L5 clouds appear to be compositionally indistinguishable. Tentative models of the surface composition, based on the Hapke theory, are presented and discussed.

Keywords: Asteroids; Photometry; Spectroscopy

1. Introduction

Beyond the asteroid main belt, in the Jupiter Lagrangian points L4 and L5, there are two clouds of small bodies of the Solar System, called Jupiter Trojans. The origin of these bodies is still far from being completely understood and several hypothesis have been so far proposed (Marzari et al., 2003; Morbidelli et al., 2005). Morbidelli et al. (2005) suggested that Jupiter Trojans, like Kuiper belt objects and the scattered disk, originated in the planetesimal disk which drove the planetary migration. Before being captured in the region where they are still observable, Jupiter Trojans had temporarily large eccentricity that brought them relatively close to the Sun, where cometary activity should have been intense. Although the scenario of their formation has not been definitively assessed, it is widely accepted that Jupiter Trojans formed at large heliocentric distances, in a region rich in frozen volatiles. Moreover, they are widely believed to have now stable orbits and to have suffered an intense collisional evolution. The recent discovery of dynamical families among Jupiter Trojans seems to support this idea.

☆ Based on observations carried out at the European Southern Observatory (ESO), La Silla, Chile, ESO proposals 69.C-0524 and 71.C-0650, and at the Telescopio Nazionale Galileo, La Palma, Canary Island, proposals TAC06 (AOT7) and TAC705 (AOT6).

* Corresponding author. Fax: +39 06 9447243.
E-mail address: dotto@mporzio.astro.it (E. Dotto).

0019-1035/$ – see front matter
doi:10.1016/j.icarus.2006.02.012

So far we know more than 1900 Jupiter Trojans. Their physical properties and their surface composition are at present not yet fully understood. Visible and near-infrared spectra are available for a limited sample of these objects (Jones et al., 1990; Jewitt and Luu, 1990; Luu et al., 1994; Fitzsimmons et al., 1994; Lazzarin et al., 1995; Dumas et al., 1998; Emery and Brown, 2001, 2003; Bendjoya et al., 2004; Fornasier et al., 2004a). The main characteristics are featureless spectra, low albedo and red colors: the large majority of them belongs to the D taxonomic class but P- and C-types are also present among them.

Although Jupiter Trojans are believed to have formed in a region rich in frozen volatiles, water ice is still undetected in their spectra. A large part of the infrared spectra of Jupiter Trojans available in the literature has been recently published by Emery and Brown (2004) who obtained 0.3–4.0 μm spectra of 17 bodies and presented also models of the surface composition. They did not detect water ice and hydrated silicate features in their V–NIR spectra and they estimated upper limits of a few percents and up to 30%, respectively, for these materials at the surface. To explain this lack of water ice on the surface of the observed objects, space weathering mechanisms can be invoked. Laboratory experiments have shown that solar wind, high-energy particles and microimpacts can alter icy surfaces of atmosphereless bodies, producing an irradiation mantle spectrally red and with low albedo (Moore et al., 1983; Thompson et al., 1987; Strazzulla, 1998; Hudson and Moore, 1999). However, if Jupiter Trojans experienced a phase of cometary activity water ice on their surface could have been devolatized early in their history, when they went through the high eccentricity phase. Alternatively, they could have formed a dust mantle as shown by Tancredi et al. (2006) for large comets (a few km-size comet nuclei). As a consequence, water ice, originally present on the surface of Jupiter Trojans, would be now completely covered and still present only in their interiors. In this scenario ice signatures could be detectable only if recent collisions would expose inner fresh material.

In order to increase the available sample of visible and near-infrared spectra of Jupiter Trojans and to investigate the surface composition of these objects, we started in 2002 an observational program at the European Southern Observatory (ESO, Chile), using both the New Technology Telescope (NTT) and the Very Large Telescope (VLT), and at the 3.6-m Telescopio Nazionale Galileo (TNG, La Palma, Spain). The sample selection done by the other teams which studied the physical properties of Jupiter Trojans was not based on dynamical constraints. On the contrary, we concentrated on members of dynamical families, as defined by Beaugé and Roig (2001), with the aim to look for the presence of water ice on their surfaces. In fact, the collisional disruptions which are supposed to have produced dynamical families might have exposed on the surface of the fragments some of the ices originally present in the interior of the parent body. Therefore, water ice likely present in the interior of larger Trojans, might be observable on the surfaces of the family members if the family formation is somewhat recent.

2. Observations

We carried out visible and near-infrared spectroscopy and photometry of Jupiter Trojans belonging to different dynamical families. We selected our targets from a list kindly provided by Beaugé and Roig (personal communication) as an update of the list by Beaugé and Roig (2001) and P.E.Tr.A. Project at www.daf.on.br/froig/petra/. In particular our selection was based on a cutoff threshold $Q = 0.014$ (Q is the upper limit of a metric so that a cluster be significant), corresponding to relative velocities of about 180 m/s.

Simultaneous visible and near-infrared spectroscopic and photometric observations of the L5 cloud have been carried out during 3 nights on November 2002 from ESO-NTT and ESO-VLT telescopes. Additional near-infrared spectroscopic observations have been performed at the TNG telescope during 3 nights on November–December 2002. From ESO-NTT and ESO-VLT we observed six objects belonging to the dynamical families of Aneas (1172 Aneas, 15502 1999 NV27, and 18493 1996 HV9) and Astyanax (1871 Astyanax, 23694 1997 KZ3, and 30698 Hippokoon). From the TNG we obtained near-infrared spectra of five objects belonging to the dynamical families of Sarpedon (2223 Sarpedon and 5130 Ilioneus) and Phereclos (2357 Phereclos, 6998 Tithonus and 18940 2000 QV49).

The L4 cloud has been observed on April–May 2003. Simultaneous visible and near-infrared spectroscopic and photometric observations have been carried out during 3 nights on April 2003 from ESO-NTT and ESO-VLT, acquiring data on six members of the Makhaon family (12917 1998 TG16, 13463 Antiphos, 15094 1999 WB2, 15535 2000 AT177, 20738 1999 XG191, 24390 2000 AD177). Further non-simultaneous visible and near-infrared spectroscopic observations have been carried out from TNG during 3 nights on May 2003, observing eight objects, members of the dynamical families Makhaon (12921 1998 WZ5, 20738 1999 XG191), 1986 WD (4035 1986 WD, 6545 1986 TR6, 11351 1997 TS25), and Menelaus (1647 Menelaus, 5244 Amphilochos, 5258 1989 AU1).

All the observations have been carried out in visitor mode.

The circumstances of the photometric and spectroscopic observations are reported in Appendix A, Tables A.1–A.7.

2.1. Visible spectroscopy and photometry

2.1.1. ESO-NTT visible observations

In November 2002 and April 2003 visible observations carried out at the ESO-NTT telescope were performed simultaneously to the ESO-VLT near-infrared observations. During these observing runs we performed both photometric and spectroscopic observations. Visible data of L5 Trojans obtained on November 2002 have been already published by Fornasier et al. (2004a).

The broadband B, V, R, and I photometric data of each target observed on April 2003 were obtained just before the spectral observations (Table 1). We used the RILD mode of EMMI for wide field imaging with the broadband B, V, R, and I filters, centered respectively at 4139, 5426, 6410, and 7985 Å. The

Table 1
Visible photometric observations of L4 Trojans (ESO-NTT EMMI): for each object, date, computed V magnitude, B–V, V–R, and V–I colors are reported

Object	Date	UT	V	B–V	V–R	V–I
12917	10 Apr. 03	00:30	18.835 ± 0.031	0.724 ± 0.042	0.537 ± 0.042	0.947 ± 0.055
13463	11 Apr. 03	00:38	18.239 ± 0.032	0.692 ± 0.045	0.449 ± 0.034	0.861 ± 0.057
15094	11 Apr. 03	06:08	19.123 ± 0.053	0.652 ± 0.065	0.477 ± 0.065	0.799 ± 0.068
15535	10 Apr. 03	07:51	17.843 ± 0.031	0.727 ± 0.041	0.495 ± 0.042	0.913 ± 0.055
15535	10 Apr. 03	08:26	17.831 ± 0.031	0.751 ± 0.042	0.446 ± 0.042	0.950 ± 0.055
20738	10 Apr. 03	04:56	18.749 ± 0.031	0.776 ± 0.041	0.472 ± 0.042	0.939 ± 0.055
24390	11 Apr. 03	03:23	18.815 ± 0.032	0.700 ± 0.042	0.513 ± 0.034	0.975 ± 0.057

The given UT is relative to the V filter acquisition. The observing photometric sequence (V–R–B–I) took a few minutes.

observations were carried out in 2×2 binning mode, yielding a pixel scale of 0.33 arcsec/pixel. Several standard stars (Landolt, 1992) have been observed over a wide range of airmasses and stellar types. The CCD images were reduced and calibrated with a standard method. First, bias and flat-field corrections were performed: a master flat field was obtained as a median of several flat fields obtained during twilight. Then the instrumental magnitudes have been computed, together with zero point, extinction and color terms necessary to convert instrumental magnitudes to apparent magnitudes. The final colors are reported in Table 1. The error bars take into account both the instrumental errors, given by photon statistics alone, and the calibration errors. By visual inspection no coma was detected for any of the observed objects.

Visible spectroscopy has been performed at ESO-NTT on April 2003 using the grism #7 (150 g/mm) in the RILD arm of EMMI, covering the spectral range 5200–9600 Å, with a dispersion of 3.6 Å/pixel at the first order. Spectra were taken through a 1 arcsec wide slit oriented along the parallactic angle in order to avoid flux loosing due to the atmospheric diffraction. Appendix A, Table A.1 reports the circumstances of these observations. Bias, flat-field, calibration lamp (He–Ar) and several (6–7) solar analog stars spectra have been recorded during each night. Spectra were reduced with the software packages Midas and IDL using standard procedures (see Fornasier et al., 2004a) which include: subtraction of the bias from the raw data, flat field correction, cosmic rays removal, background subtraction, collapsing the two-dimension spectra to one-dimension, wavelength calibration and atmospheric extinction correction (using La Silla atmospheric extinction coefficients). Wavelength calibration was made using a lamp with He and Ar emission lines. The reflectivity of the asteroids was then obtained by dividing their spectra by the spectrum of the solar analog star the closest in time and airmass to the object, as reported in Appendix A, Table A.1. Finally, spectra have been smoothed with a median filter technique, using a box of 19 pixels.

2.1.2. TNG visible observations

Visible spectroscopy has been acquired at the TNG telescope on May 2003. We used the DOLORES (Device Optimized for the LOw RESolution) instrument equipped with the low resolution red grism (LR-R) covering the 0.51–0.98 μm range with a spectral dispersion of 2.9 Å/pixel (http://www.tng.iac.es). During the observing run we also acquired bias, flat-field, calibration lamp (Ne–Ar lines) and several solar analog spectra. For all the targets, with the exception of 11351, the total exposure time was divided into 2 acquisitions of respectively 10 min. This allowed us also to check the asteroid position inside the slit before each acquisition and to reduce the cosmic rays hits on each spectrum. For data reduction we followed the same procedure applied for the NTT spectra. Appendix A, Table A.2 reports the observational circumstances of these observations.

2.2. Near-infrared spectroscopy and photometry

2.2.1. ESO-VLT near-infrared observations

To perform near-infrared photometry and spectroscopy at ESO-VLT we used the first Unit Telescope (UT1, Antu) equipped with the infrared-cooled grating spectrometer ISAAC (Infrared Spectrometer And Array Camera) (www.eso.org/instruments/isaac) and with a Rockwell Hawaii 1024×1024 pixel Hg:Cd:Te array. Photometric J, H, and Ks measurements (centered at 1.25, 1.65, and 2.2 μm) have been performed before and after the spectra. The details of the near-infrared photometric observations are reported in Appendix A, Tables A.3 and A.4. Near-infrared photometry has been carried out using the jitter imaging technique: a combined image is generated with the jitter routine from the ECLIPSE package. The used data processing routines are described in Dotto et al. (2003a) and Romon et al. (2001). The calibration was performed by the observation of several faint infrared standard stars from Hunt et al. (1998) and Persson et al. (1998). Final colors are reported in Table 2.

Spectroscopic observations were performed in the SW mode (1–2.5 μm wavelength range). We used the ISAAC low resolution spectroscopic mode with a 1 or 1.5 arcsec wide slit and the grating at three different central wavelengths corresponding to J, H, and K bands (Appendix A, Table A.5). The pixel scale is 0.147 arcsec/pixel. We observed separately the three spectral ranges (J, H, and K) corresponding to 1.10–1.39, 1.42–1.83, and 1.84–2.56 μm. The final spectral resolution for the 1 arcsec slit is 500 for the J and H bands and 450 for the K band. The observations were done by nodding the object along the slit by 10 arcsec between two positions A and B. The two averaged A and B images in each spectral range (J, H, and K) were subtracted from each other. The A–B and B–A images were flat-fielded, corrected for spatial and spectral distortion and finally combined with a 10-arcsec offset. The spectra were extracted from the resulting combined images, and wavelength calibration was performed using xenon–argon lamp spectra. The telluric ab-

Table 2
V magnitude and color indices of family Trojans

Object	V	J	H	K	V–J	J–K	H–K
L5							
1172	16.174 ± 0.020	14.597 ± 0.030	14.167 ± 0.030	14.032 ± 0.020	1.577 ± 0.030	0.565 ± 0.040	0.135 ± 0.030
1871	18.379 ± 0.034	16.848 ± 0.036	16.510 ± 0.036	16.391 ± 0.020	1.531 ± 0.050	0.457 ± 0.030	0.119 ± 0.030
1871	18.379 ± 0.034	16.888 ± 0.036	16.540 ± 0.036	16.388 ± 0.020	1.491 ± 0.050	0.500 ± 0.030	0.153 ± 0.030
1871	18.293 ± 0.027	16.949 ± 0.027	16.532 ± 0.027	16.429 ± 0.016	1.344 ± 0.040	0.520 ± 0.022	0.103 ± 0.022
15502	17.061 ± 0.023	15.523 ± 0.032	15.031 ± 0.032	14.876 ± 0.020	1.538 ± 0.040	0.647 ± 0.025	0.155 ± 0.025
15502	17.061 ± 0.023	15.457 ± 0.023	14.964 ± 0.024	14.817 ± 0.015	1.604 ± 0.030	0.640 ± 0.018	0.147 ± 0.019
18493	18.298 ± 0.023	16.898 ± 0.036	16.520 ± 0.036	16.445 ± 0.020	1.400 ± 0.040	0.453 ± 0.030	0.075 ± 0.030
18493	18.393 ± 0.022	17.022 ± 0.029	16.633 ± 0.029	16.528 ± 0.017	1.371 ± 0.040	0.494 ± 0.023	0.105 ± 0.023
23694	18.593 ± 0.024	16.936 ± 0.023	16.443 ± 0.024	16.232 ± 0.015	1.657 ± 0.030	0.704 ± 0.018	0.211 ± 0.019
30698	19.244 ± 0.035	17.757 ± 0.053	17.322 ± 0.053	17.140 ± 0.035	1.487 ± 0.060	0.617 ± 0.040	0.182 ± 0.040
30698	19.244 ± 0.035	17.680 ± 0.050	17.319 ± 0.044	17.135 ± 0.060	1.465 ± 0.060	0.545 ± 0.078	0.184 ± 0.074
L4							
12917	18.835 ± 0.031	17.128 ± 0.058	16.653 ± 0.064	16.448 ± 0.050	1.707 ± 0.066	0.680 ± 0.076	0.205 ± 0.081
13463	18.239 ± 0.032	16.822 ± 0.036	16.479 ± 0.042	16.376 ± 0.030	1.417 ± 0.048	0.446 ± 0.046	0.103 ± 0.051
15094	19.123 ± 0.033	17.764 ± 0.036	17.422 ± 0.050	17.327 ± 0.030	1.359 ± 0.051	0.437 ± 0.046	0.095 ± 0.058
15535	17.843 ± 0.031	16.156 ± 0.032	15.656 ± 0.036	15.533 ± 0.030	1.687 ± 0.045	0.623 ± 0.044	0.123 ± 0.047
15535	17.831 ± 0.031	16.156 ± 0.032	15.656 ± 0.036	15.533 ± 0.030	1.675 ± 0.045	0.623 ± 0.044	0.123 ± 0.047
20738	18.749 ± 0.031	17.156 ± 0.054	16.636 ± 0.064	16.523 ± 0.050	1.593 ± 0.062	0.633 ± 0.073	0.113 ± 0.081
24390	18.815 ± 0.032	17.131 ± 0.036	16.670 ± 0.042	16.530 ± 0.030	1.684 ± 0.048	0.601 ± 0.047	0.140 ± 0.051

sorption correction and the removal of the solar contribution were obtained dividing the spectra of the asteroids by those of different solar analog stars, observed at similar airmasses. The resulting spectra were smoothed with a median filtering technique. The edges of each spectral region have been cut to avoid low S/N spectral regions.

2.2.2. *TNG near-infrared observations*

Near-infrared spectroscopic data, non-simultaneous to the visible observations, have been carried out on November 2002 and May 2003 with the 3.6-m TNG telescope at La Palma (Appendix A, Tables A.6 and A.7). We used the Near-Infrared Camera and Spectrometer (NICS), a FOSC-type cryogenic focal reducer, equipped with two interchangeable cameras feeding a Rockwell HgCdTe Hawaii 1024 × 1024 pixel array. NICS was used in its low-resolution spectroscopic mode and equipped with an Amici prism disperser, which allowed us to obtain a continuous spectrum in the wavelength range 0.8–2.4 μm. A slit of 1.5 arcsec was used, providing a final spectral resolution of 34. The pixel scale is 0.25 arcsec/pixel. Also in this case, the observations were carried out by offsetting the telescope by 30 arcsec in the direction of the slit between two different positions A and B. Several A and B images of 60-, 90-, and 120-s individual exposure time were obtained to avoid saturation. Reduction of the spectra was done by subtracting consecutive A and B images and applying the procedure already used by Licandro et al. (2002). Both 2002 and 2003 observing runs were carried out in non-photometric conditions, and the composite visible and near infrared spectra have been obtained by overlapping the spectral interval between 0.8 and 0.9 μm which is common to NICS and DOLORES. The wavelength calibration has been performed following the NICS manual, using a look-up table which is based on the theoretical dispersion predicted by ray-tracing and adjusted to best fit the deep telluric absorption features. The resolution given by the instrument is in fact so low, that all the Ar–Xe lines are blended and cannot be easily used for standard reduction procedures.

Each asteroid spectrum has been reduced vs each solar analog and normalized at 1.6 μm. Considering that the spectra of the solar analogs divided by each other were very similar with differences in slope smaller that 0.4%/1000 Å, the final asteroid spectra have been computed averaging the spectra of each object divided by different solar analogs (see Appendix A, Tables A.6 and A.7). Finally, the composite visible and near infrared spectrum for each asteroid has been obtained scaling the infrared spectra in order to be attached to the visual part (normalized to 5500 Å).

3. Spectral analysis and surface modeling

Figs. 1 and 2 show the whole sample of visible spectra obtained at the TNG telescope and at the ESO-NTT telescope.

Figs. 3–6 show the visible and near-infrared spectra obtained for each dynamical family. For observations carried out at ESO, where the photometric calibration has been performed, the different spectral ranges have been adjusted using the computed color indices. For TNG observations the photometric calibration was not possible. In any case they are not needed as visible and near-infrared spectra have an overlapping region between 0.80–0.95 μm. The values and slopes of visible and near-infrared spectra in this spectral region have been used to adjust them. For the L5 family members our near-infrared spectra are shown along with the visible spectra published by Fornasier et al. (2004a).

We estimated the diameter of 19 of our targets, with the exception of 1172, 2223, 2357, 1647, 4035 whose diameters have

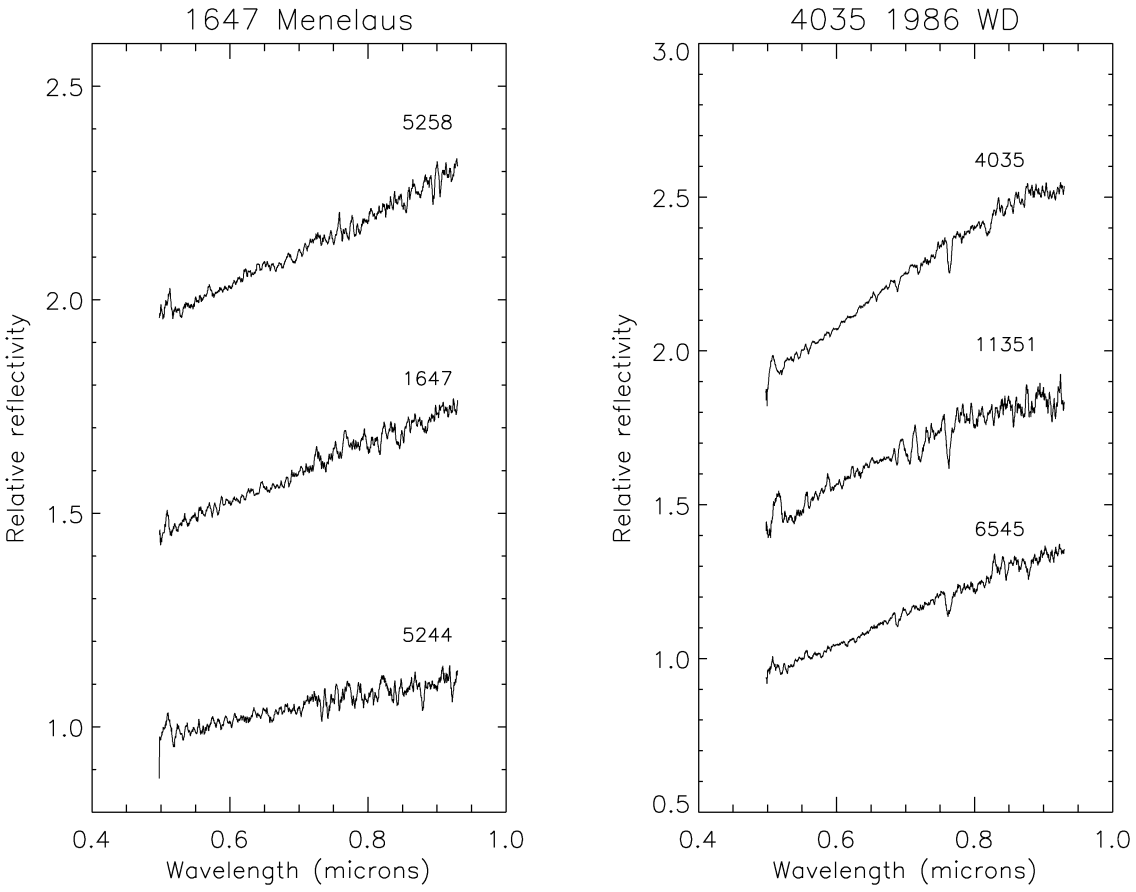

Fig. 1. Visible spectra of the L4 Trojans belonging to the Menelaus and 1986 WD families, obtained at TNG on May 2003. All the spectra are normalized to 1 at 0.55 μm and shifted by 1 in reflectance for clarity.

been taken from the IRAS data. We used the V magnitudes here presented (Table 1) and those already published by Fornasier et al. (2004a) to compute the absolute magnitudes H applying the (G, H) model by Bowell et al. (1989)

$$H = \mathrm{V} - 5\log(r\Delta) + 2.5\log\Big\{(1-G)\exp\big[-3.33\tan^{0.63}(\alpha/2)\big] + G\big[-1.87\tan^{1.22}(\alpha/2)\big]\Big\},$$

where V is the observed magnitude, r and Δ are the heliocentric and geocentric distances (in AU), respectively, α is the phase angle, and G is the slope parameter assumed of 0.05 in agreement with Fernandez et al. (2003). For the 7 objects observed at TNG (1647, 4035, 5244, 5258, 6545, 11351, 12921), for which we do not have visible photometric data, we rely upon the Lowell Observatory absolute magnitudes, derived from the astorb.dat file. Diameters D have been computed from the absolute magnitudes H and the albedos p as

$$D = \frac{1329 \times 10^{-H/5}}{\sqrt{p}}$$

assuming an albedo range of 0.03–0.07, with a mean value of 0.04 (Fernandez et al., 2003; Jewitt et al., 2000). The obtained H and D values are reported in Table 3.

To interpret the spectra of the observed Jupiter Trojans in terms of the surface composition we ran a radiative transfer model, based on the Hapke theory and already applied to centaurs and trans-neptunian objects (Barucci et al., 2002; Dotto et al., 2003a, 2003b, 2003c; de Bergh et al., 2004; Fornasier et al., 2004b). We considered several compounds that are expected to be present on the surface of Trojans, taking into account that they likely formed at large heliocentric distances. In particular we considered the following materials at different grain sizes: organics solids (e.g., kerogens by Clark et al., 1993 and Khare et al., 1991; Titan tholins from Khare et al., 1984; and Triton tholins from McDonald et al., 1994), amorphous carbon (by Zubko et al., 1996), and different minerals (silicates [e.g., olivines, pyroxenes], phyllosilicates [e.g., montmorillonite, serpentine], oxides [e.g., hematite], sulfates [e.g., jarosite] and all the minerals included in the US Geological Digital Spectral Library http://speclab.cr.usgs.gov/spectral-lib.html), bitumen (by Moroz et al., 1998), and ices (H_2O, CH_4, CH_3OH, NH_3, and ice tholins by McDonald et al., 1996, and Khare et al., 1993). Several geographical (spatially segregated) mixtures of all these compounds have been modeled and for each combination synthetic spectra were compared with the observed ones. The constraints to be satisfied were: low albedo, visible spectral slope, spectral behavior in the near-infrared wavelengths. Table 3 reports for each object the combination of compounds and their percentages which best reproduces the observed spectral behav-

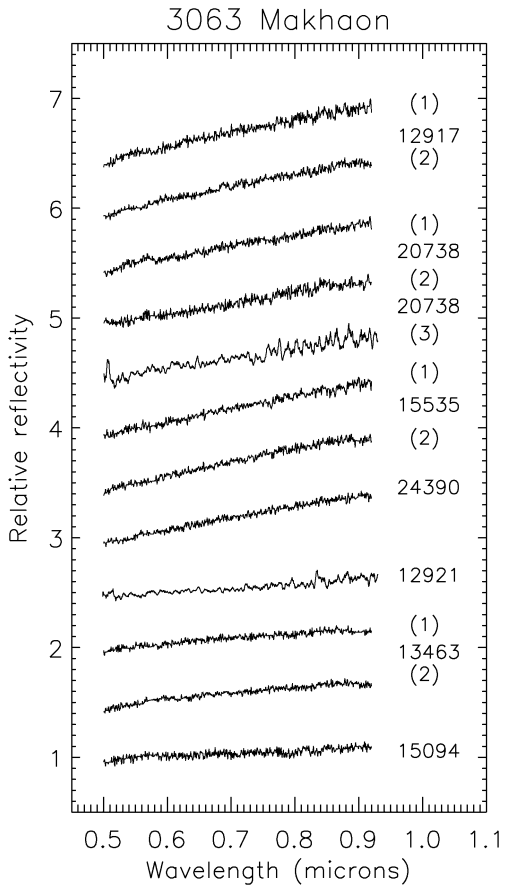

Fig. 2. Visible spectra of the L4 Trojans belonging to the Makhaon family, obtained at ESO-NTT on April 2003. Spectrum (3) of 20738 and the spectrum of 12921 have been obtained at TNG on May 2003. All the spectra are normalized to 1 at 0.55 μm and shifted by 1 in reflectance for clarity.

iors, together with the albedo values at 0.55 μm resulting from our modeling (all ranging between 0.03 and 0.06). In Table 3 we show also the IRAS albedo available for five objects (1172, 1647, 2223, 2357, and 4035). For four of these asteroids (1172, 1647, 2223, 2357) the albedos we have computed on the basis of the synthetic spectra are in agreement with the IRAS values. For 4035 we did not find a mixture of minerals able to reproduce the observed spectrum, maintaining the albedo at 0.08, a quite high value for a Jupiter Trojan. Further observations of this object are recommended in order to check the albedo and diameter computation as well as the thermal properties and the spectral behavior.

The synthetic spectra corresponding to the model of the surface composition of each target are represented in Figs. 3–6 as superimposed solid lines.

Of course the used spectral inversion method does not produce unique solution: different combinations of other minerals in different percentages and grain sizes can lead to synthetic spectra compatible with the observed ones. The spectra we obtained are featureless, no signature related to minerals or icy component has been detected. To reproduce the uniformly red spectral behavior, observed between 0.3 and 1.2 μm, we considered tholins and kerogens. Cruikshank et al. (2001) demonstrated that organic solids are not necessary to reproduce the spectral behavior of red spectra and modeled the spectrum of 624 Hektor with Mg-rich pyroxenes and serpentine. Also Emery and Brown (2004) limited the inclusion of tholins in their models of the surface composition of Trojans as they did not find in their spectra any absorption at about 3 μm. Our spectra, limited to 2.4 μm, do not allow to check the feature at 3 μm and to verify the presence of tholins on the surface of our targets. As a consequence, tholins and kerogens included in our models have to be considered only as reddening agents.

3.1. The L5 families

3.1.1. Aneas family

Five out of six members of this family were observed in the visible range by Fornasier et al. (2004a). Four of them were classified as D-types and their visible spectral slopes showed an increasing trend at decreasing sizes. One object (18493 1996 HV9) classified as P-type was out of this trend. We observed in the near-infrared region three of these objects: the two largest members of the family (1172 has a diameter of about 143 km, and 15502 has a diameter of about 68 km) and the possible interloper 18493. Fig. 3 shows the complete visible and near infrared spectra. 1172 and 15502 have very similar spectral behavior: their colors are comparable (see Tables 1 and 2) and their spectra are both reddish, suggesting that they might have common origin and composition. Their surface composition has been modeled with the same mixture of kerogens, amorphous carbon, silicates and Titan tholins (see Table 3). On the contrary, the spectrum of 18493 is flatter than the others and the color indices are very different. Its surface composition has been modeled with a different mixture composed of a higher amount of amorphous carbon and a small percentage of organic compounds (kerogens and tholins).

Even considering that the available sample is very small, the analysis of the obtained visible and near-infrared spectra confirms that 18493 is different from the other members of Aneas. Its spectral diversity compared to 1172 and 15502 could indicate either that 18493 is an interloper or that it comes from the interior of the parent body. This last hypothesis would imply that this object has experienced during its life-time a low degree of space weathering alteration, or, alternatively, that it has a peculiar surface composition if the parent body was differentiated.

3.1.2. Astyanax family

Fornasier et al. (2004a) presented the visible spectra of 4 out of 5 members of this family and classified all of them as belonging to the D-type. We obtained simultaneous near-infrared observations of three of these members (1871, 23694, and 30698) which have similar estimated diameters (around 25–35 km). If the analysis of the visible colors and spectra suggested a quite homogeneous composition, the near-infrared spectra show very different behaviors. 1871 and 30698 have similar colors and moderately red spectra, while 23694 exhibit a slope in the infrared range steeper than the other two family members. To reproduce the observed spectral behaviors we considered sev-

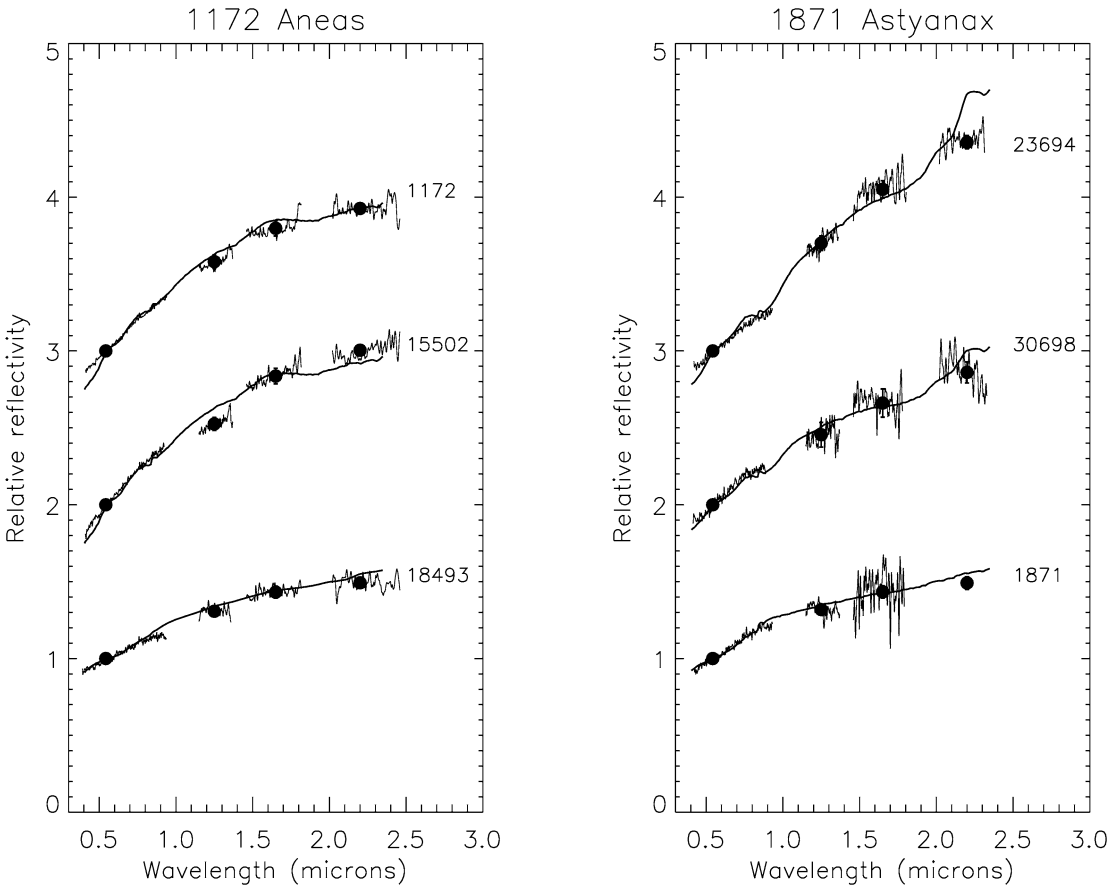

Fig. 3. Near-infrared spectra of L5 Trojans belonging to the Aneas and Astyanax families obtained at ESO-VLT on November 2002, together with the visible part already published by Fornasier et al. (2004a). All the spectra are normalized to 1 at 0.55 μm and shifted by 1 in reflectance for clarity. The superimposed continuous lines represent the synthetic spectra obtained modeling the surface composition.

eral combinations of minerals. The synthetic spectra reported in Fig. 3 have been obtained considering different combinations of amorphous carbon, small amounts of silicates and organic compounds (see Table 3). From the spectrally flattest to the spectrally reddest object the percentage of amorphous carbon decreases while the percentage of organics increases, giving a higher albedo value. Further observations of all the family members would be necessary to investigate the reliability of Astyanax family and the composition and structure of the parent body.

3.1.3. *Sarpedon family*

All 4 members of this family were observed in the visible range by Fornasier et al. (2004a). This is a strong cluster from the dynamical point of view and all the objects were classified as belonging to the D-type. We observed the two larger members (2223 and 5130) also in the near-infrared range, obtaining the 0.4–2.4 μm spectra reported in Fig. 4. The visible part in this case was not simultaneously acquired to the near-infrared one. Visible spectra of 2223 and 5130 are very similar each other, while the near-infrared behavior is quite different. The suggested surface compositions are constituted by different mixtures of amorphous carbon, tholins and kerogens. From our proposed compositional models 2223 seems to contain some percentage of silicates and a larger amount of tholins, while 5130 was modeled with kerogens, amorphous carbon, and a few percentages of Triton tholins (see Table 3). Observations of more members are absolutely needed to constrain the homogeneity of the family and, as a consequence, the nature of the parent body.

3.1.4. *Phereclos family*

The Phereclos cluster contains 6 members at a cutoff level of $Q = 0.014$. We observed 3 of them in the near-infrared range (Fig. 4). These spectra are quite different from each other, confirming the diversity already reported by Fornasier et al. (2004a) from visible spectroscopy. The models of the surface composition of 6998 and 18940 contain different percentages of amorphous carbon, kerogens, and tholins. The spectrum of 2357, the largest member of the family, is redder up to 1.6 μm, suggesting a surface rich in tholins and containing a few percents of silicates.

3.2. *The L4 families*

3.2.1. *Menelaus*

Menelaus is a very huge cluster, surviving up to a cutoff of 100 m/s, of which we observed only three members (Fig. 5).

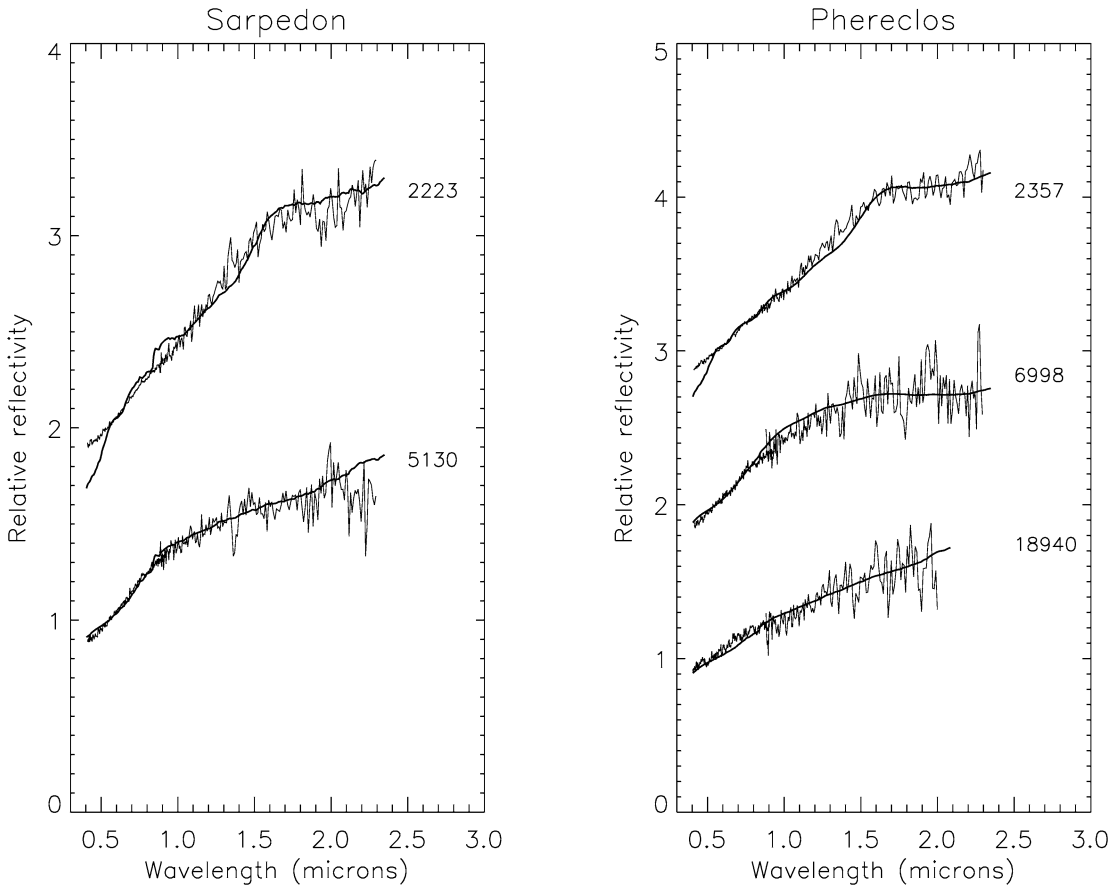

Fig. 4. Near-infrared spectra of L5 Trojans belonging to the Sarpedon and Phereclos families obtained at TNG on November–December 2002, together with the visible part already published by Fornasier et al. (2004a). All the spectra are normalized to 1 at 0.55 μm and shifted by 1 in reflectance for clarity. The superimposed continuous lines represent the synthetic spectra obtained modeling the surface composition.

The obtained spectra show a continuous trend with increasing spectral slope from 5244 and 5258. Since the spectral behaviors are very similar, this spread can be interpreted as due to different levels of space weathering processing. The compositional models that reproduces the spectral behavior of these members (see Table 3) are very similar to each other, being composed by a mixture of a high percentage of amorphous carbon and few percent of tholins: from 2% in the case of 5244 to 6% in the case of 5258.

3.2.2. *1986 WD*

This cluster includes 6 members at a cutoff of 0.010, corresponding to a relative velocity of the order of 130 m/s. We carried out non-simultaneous visible and near-infrared observations of 3 of them and the obtained 0.4–2.4 μm spectra are shown in Fig. 5. All the objects have similar spectral behaviors: the visible spectrum of 4035, the biggest member of the family, is slightly redder than the visible spectra of the other two observed objects, and this difference is evident also in the whole 0.4–2.4 μm spectra. As a consequence the compositional models are quite different: the surfaces of 6545 and 11351 are modeled with the same combination of kerogens, amorphous carbon and tholins, while the percentages of tholins increases in the model of 4035 to better reproduce its redder spectral slope. In any case the cluster seems to be quite homogeneous, even if the observational sample need to be extended to the whole family to give an insight of its nature and of the possible structure of the parent body.

3.2.3. *Makhaon family*

Makhaon is a very strong dynamical family which survives up to a cutoff of 100 m/s. We observed all the 7 members present at a cutoff of $Q = 0.10$ corresponding to a relative velocity of the order of 130 m/s. Among these objects 12917, 12921, 20738, and 15535 represent a strong core of the family, surviving up to values of the relative velocities around 100 m/s. The obtained visible and near-infrared spectra are shown in Fig. 6. They present a continuous range of variation, starting from 15094 which could be classified as a C-type, up to 12917, 15535, 20738, and 24390 which show very similar red spectra. These four objects have similar dimensions (between 29 and 48 km) and show very similar spectral behaviors. Small differences in spectral slope can be, also in this case, attributed to different level of space weathering processing of their surfaces. In the new version of the member lists of Jupiter dynamical families (www.daf.on.br/froig/petra/families.htm) 15094 is no more included in this family and 13463 appears only at a cutoff of 130 m/s. On the basis of this consideration we can assume

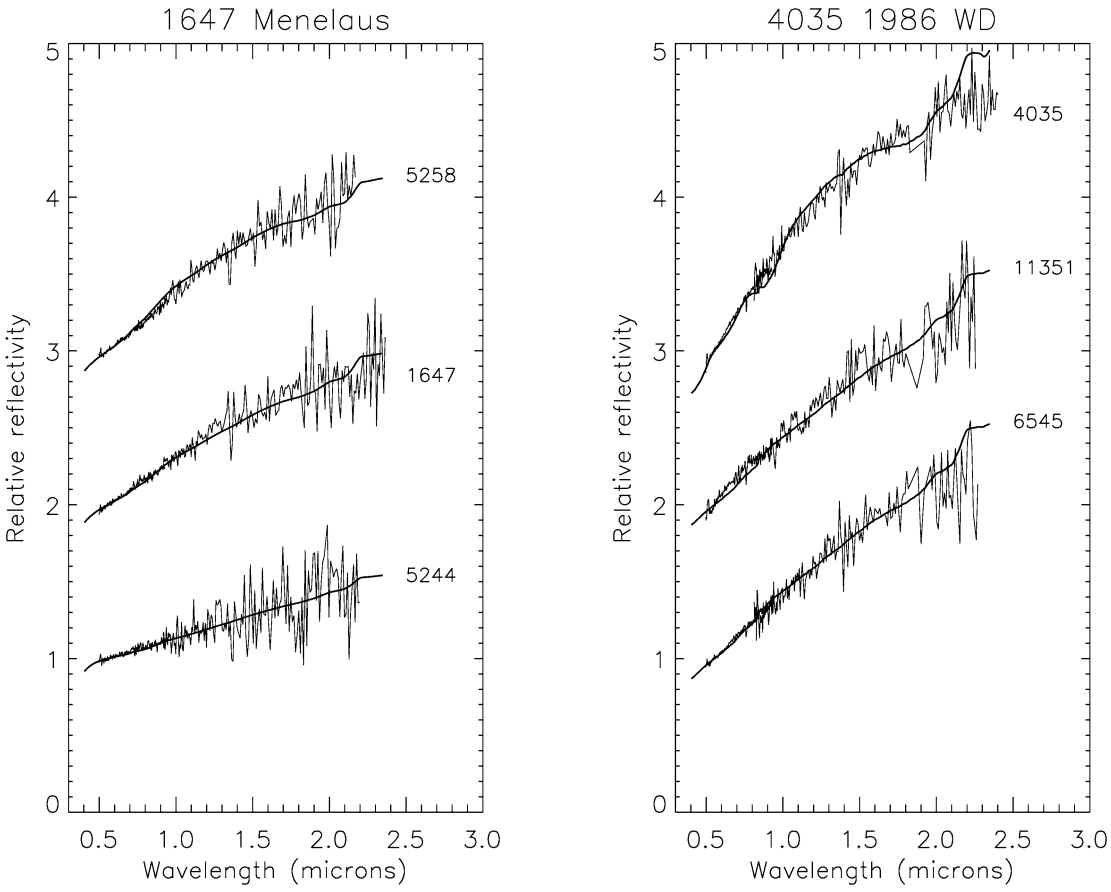

Fig. 5. Visible and near-infrared spectra of L4 Trojans belonging to the Menelaus and 1986 WD families obtained at TNG on May 2003 All the spectra are normalized to 1 at 0.55 μm and shifted by 1 in reflectance for clarity. The superimposed continuous lines represent the synthetic spectra obtained modeling the surface composition.

that these two objects, which have the flattest spectra shown in Fig. 6, could be interlopers in our sample. The obtained models (see Table 3) are very similar to each other, being composed by a mixture of a high percentage of amorphous carbon and kerogens with few percents of tholins, with the amount of this latter slightly increasing with the increasing of the spectral slope.

4. Discussion

A strong homogeneity of the Trojan population is the main characteristic we derived from our survey. Most of the observed Trojans family members appear to belong to the P–D taxonomic type. No diagnostic spectral signatures have been found to distinguish a family with respect to the others. All the observed spectra have been modeled with a surface composition given by mixtures of amorphous carbon and organic compounds with small percentages of silicates. Different slopes in the region 0.5–1.2 μm, probably due to different degrees of space weathering, have been reproduced with mixtures of different percentages of organic compounds which redden the spectra, without changing neither the albedo value, nor the nature of the surface composition. As discussed by Cruikshank et al. (2001) and Cruikshank and Dalle Ore (2003), organic compounds are only one possibility to model low-albedo surfaces having spectra as red as the Jupiter Trojans, but they are not essential for this kind of models. Other mineral mixtures, e.g., Mg-rich pyroxene and serpentine as used in the case of Hektor, can produce spectra similar to those of Jupiter Trojans. Since in our spectra we cannot check the presence of the tholin spectral feature at about 3 μm, we cannot affirm the presence of tholins on the surface of the observed targets, but we can consider them as possible reddening agents allowing us to reproduce the slope observed between 0.5 and 1.2 μm.

We investigated also the possible relations between spectral slopes, color indices and dynamical characteristics. We computed the difference between the reflectance at 0.85 μm (corresponding approximately to the center of the x filter in the ECAS survey) and at 2.2 μm (corresponding to the K color) for all the 24 investigated Trojans to obtain the x–K color index. The choice of this wavelength range allows us to include in the data set also the results on the 0.85–2.2 μm color index of 16 Trojans presented by Emery and Brown (2004, Table 4). Considering that Asteroid 1172 Aneas was observed both by us and Emery and Brown (2004), with results quite in agreement (x–K values respectively of 1.14 ± 0.04 and 1.25 ± 0.03) we can investigate the (x–K) color index for a total sample of 39 Trojans. We analyzed the x–K color index distribution versus different proper elements (eccentricity, inclination and frequency of libration), but no relationships have been found

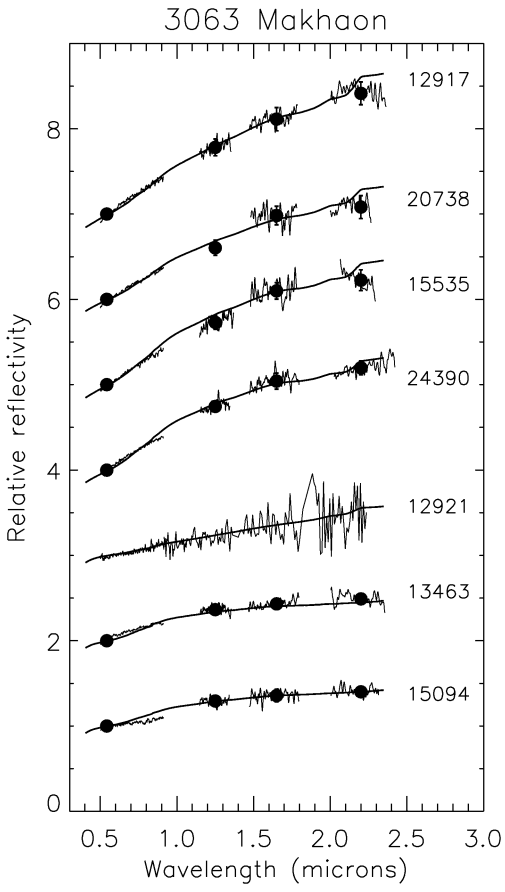

Fig. 6. Visible and near-infrared spectra of L4 Trojans belonging to the Makhaon family (ESO-NTT& VLT, TNG telescopes data). All the spectra are normalized to 1 at 0.55 μm and shifted by 1 in reflectance for clarity. The superimposed continuous lines represent the synthetic spectra obtained modeling the surface composition.

with these dynamical elements. The distribution of the x–K vs B–V and V–R color indices is shown in Fig. 7 and does not exhibit a clear trend. Trojans with low B–V color index have also a small value of the x–K color, but for higher B–V color values we see a high dispersion in the infrared colors. Objects with a high V–R color index also have high x–K value, but Trojans with lower V–R color index show a high variety in the x–K color index.

As shown in Fig. 7, the whole sample of objects has quite similar spectral characteristics and as a consequence appears to be quite homogeneous in surface composition. No differences have been found in the spectral slopes between Trojans belonging to the L4 and L5 clouds. In fact the 26 L4 Trojans analyzed have a mean x–K color $= 1.16 \pm 0.16$, while the 13 L5 Trojans have a mean x–K color 1.12 ± 0.12, therefore there are no differences within the uncertainties.

Analyzing the x–K color as a function of the diameter (see Fig. 8), we find that both small objects (diameter <80 km) and large ones have similar mean x–K values (1.12 ± 0.16 and 1.18 ± 0.11, respectively). Larger bodies have a lower dispersion in the x–K color index as compared to smaller ones. This characteristics can be interpreted as possibly due to different degrees of space weathering alteration: larger family members probably show an ageing coming in part from the parent body, while smaller fragments can came indifferently from the interior or the surface of the parent body and exhibit different degrees of space weathering alteration.

The most important result of our modeling is that none of the observed objects show the presence of spectral features at 1.5 and 2 μm, related to the presence of water ice. This is surprising, since Trojans formed beyond the snow line and the early temperatures in the protoplanetary disk were probably low enough to allow water ice condensation during their formation. The lack of detection of water ice, which is expected to be constituent of Trojans, might be due to the formation of a thick irradiation mantle on their surfaces by solar ultraviolet radiation and cosmic ray bombardment. These space weathering processes could have altered the surface properties of the reddest family members causing a reddening of the spectral slope (and a consequent darkening of the surface) as a consequence of chemical modification and the formation of complex organic materials. Alternatively, the water ice originally present on the surface of Jupiter Trojans could have been covered or removed after the cometary activity suggested by Morbidelli et al. (2005). The observations of short-periodic comets available in the literature evidence that they do not show water ice absorption features either. Only very few spectra of comets—also from spacecraft—exist, but no water ice is found on these objects down to the level of a few percent, although there is not doubt that water should exist in comets, actually as a major constituent. As a consequence, one could argue that water ice is just evaporated from the surface when they become active, or that the cometary surface is now covered by a dust mantle as shown by Tancredi et al. (2006) in the case of large comets (a few km-size comet nuclei).

In conclusion, the Trojans' surface could be covered by a dust or irradiation mantle which could inhibit the detection of water ice. Nevertheless, on the basis of the available data sample, we cannot check if water ice is present but covered by darker materials which reduce its spectral features. Further observations are needed to investigate the mechanisms which alter water ice or inhibit the detection of its signatures.

5. Conclusion

In this paper we present visible and near-infrared data of 24 Jupiter Trojans belonging to seven different families. Absolute magnitudes have been computed for 17 objects and an estimation of the diameter has been presented for 19 bodies. Tentative models of the surface composition of the whole sample of observed targets have been obtained by applying a radiative transfer model based on the Hapke theory. We considered several mixtures of minerals, and organic and icy compounds which are supposed to be present on the surface of objects at large heliocentric distances. The presented models, although not unique, can help us to investigate the nature of the observed targets, giving an insight of the surface composition of the members of each family and on the structure (homogeneity/heterogeneity) of the parent bodies.

Table 3
Absolute magnitudes (H), estimated diameters (D), models of the surface composition and albedo values at 0.55 μm resulting from modeling

Object	H	D (km)	Model	Albedo
Aneas:				
1172	8.54	143^{+5}_{-5}*	36% KE, 55% AC, 5% Tit. th., 2% Ol, 2% Ens	0.04[a]
15502	9.94	68^{+10}_{-16}	36% KE, 55% AC, 5% Tit. th., 2% Ol, 2% Ens	0.04
18493	10.78	46^{+7}_{-11}	4% KE, 94% AC, 2% Ol, 2% Ens	0.03
Astyanax:				
1871	11.29	37^{+6}_{-9}	23% KE, 76% AC, 1% Tr. th.	0.03
23694	11.59	32^{+5}_{-8}	30% KE, 55% AC, 12% Tit. th., 3% Ens	0.04
30698	12.23	24^{+4}_{-6}	29% KE, 64% AC, 5% Tit. th., 2% Ens	0.04
Sarpedon:				
2223	9.25	95^{+4}_{-4}*	70% KE, 21% AC, 4% Ol, 5% Tit. th.	0.04[b]
5130	9.85	71^{+11}_{-18}	33% KE, 65% AC, 2% Tr. th.	0.03
Phereclos:				
2357	8.86	95^{+4}_{-4}*	13% KE, 75% AC, 4% Ol, 8% Tit. th.	0.05[c]
6998	11.43	34^{+5}_{-8}	8% KE, 89% AC, 3% Tit. th.	0.03
18940	11.81	29^{+4}_{-7}	17% KE, 80% AC, 3% Tr. th.	0.03
Menelaus:				
1647	10.3**	72^{+5}_{-5}*	95% AC, 1% Tit. th., 4% Tr. th.	0.03[d]
5244	10.1**	63^{+10}_{-15}	98% AC, 2% Tr. th.	0.03
5258	10.0**	66^{+10}_{-16}	94% AC, 2% Tit. th., 4% Tr. th.	0.03
1986 WD:				
4035	9.3**	68^{+5}_{-5}*	36% KE, 41% AC, 4% Tit. th., 14% Tr. th., 5% Ens	0.05[e]
6545	10.0**	66^{+10}_{-16}	20% KE, 73% AC, 7% Tr. th.	0.03
11351	10.5**	53^{+8}_{-13}	20% KE, 73% AC, 7% Tr. th.	0.03
Makhaon:				
12917	11.61	32^{+5}_{-8}	8% KE, 83% AC, 2% Tit. th., 7% Tr. th.	0.03
12921	10.7**	48^{+7}_{-12}	4% KE, 94% AC, 2% Tr. th.	0.03
13463	11.27	37^{+6}_{-9}	10% KE, 89% AC, 1% Tit. th.	0.03
15094	11.76	30^{+5}_{-7}	4% KE, 95% AC, 1% Tit. th.	0.03
15535	10.70	48^{+7}_{-12}	5% KE, 87% AC, 3% Tit. th., 5% Tr. th.	0.03
20738	11.67	31^{+5}_{-8}	5% KE, 88% AC, 2% Tit. th., 5% Tr. th.	0.03
24390	11.80	29^{+5}_{-7}	5% KE, 88% AC, 3% Tit. th., 4% Tr. th.	0.04

The used acronyms are: KE = kerogen, AC = amorphous carbon, Tit. th. = Titan tholins, Tr. th. = Triton tholin, Ol = olivine, Ens = enstatite. Diameters marked by ∗ are taken from IRAS data. Absolute magnitudes marked by ∗∗ are taken from the astorb.dat file of the Lowell Observatory.
[a] Albedo IRAS = 0.04 ± 0.003.
[b] Albedo IRAS = 0.034 ± 0.003.
[c] Albedo IRAS = 0.052 ± 0.003.
[d] Albedo IRAS = 0.028 ± 0.004.
[e] Albedo IRAS = 0.086 ± 0.015.

The obtained results can be summarized as follows:

- None of the observed spectra exhibit spectral features at 1.5 and 2 μm related to the presence of water ice on the surface of the observed bodies.
- All the spectra belong to the primitive taxonomic classes (P and D type) and can be reproduced by modeling the surface composition with mixtures of amorphous carbon, silicates and a reddening compound (tholins and/or kerogens). We did not detect any diagnostic feature that allows us to distinguish the family members from the background objects of the Trojan population. Some small differences in the spectral behaviors can probably be explained by different degrees of space weathering alteration.
- L4 and L5 clouds are spectrally very similar and there is no evidence of compositional difference between the Jupiter preceding and following clouds.
- All the investigated dynamical families appear quite similar in surface composition, without any peculiar difference. The Jupiter Trojan population exhibit a great uniformity.

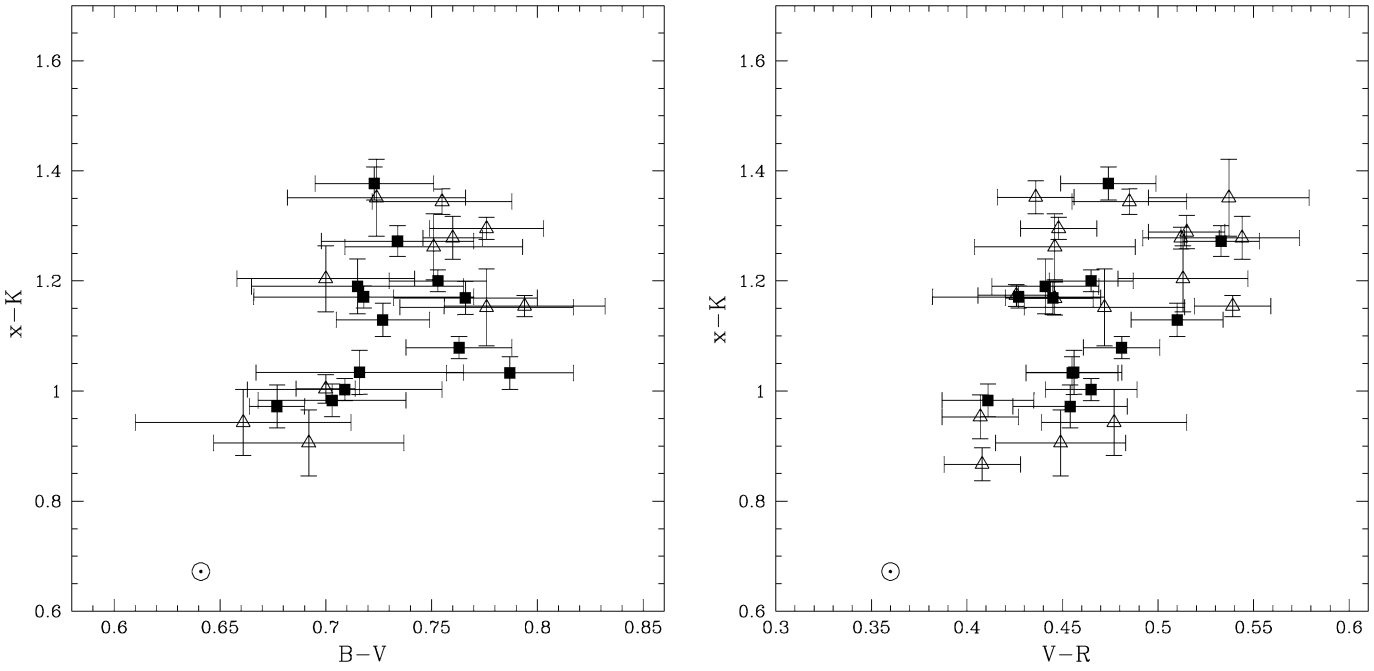

Fig. 7. The x–K color index (derived from the difference between the reflectance at 0.85 and at 2.2 μm), vs the B–V and V–R color indices for a Trojans data set composed by our data and those of Emery and Brown (2004). Open triangles correspond to data on Trojans belonging to L4 cloud, while black square are those for Trojans belonging to the L5 cloud. B–V and V–R colors have been derived directly from photometry for our NTT data, while for the TNG only data, the V–R color index has been derived from reflectance spectroscopy. B–V and V–R color indices for Emery and Brown (2004). Trojans targets have been derived from photometry or spectroscopy available in the literature, when existing (Planetary Data System—Small Bodies Data Base at http://pdssbn.astro.umd.edu/nodehtml/sbdb.html). The (x–K) color index includes the solar color both for our and Emery and Brown (2004) data. The Sun colors are represented with the ⊙ symbol.

Also for the families that show some variation among members the detected differences seem to be just random deviation within the entire population.

- The analysis of the visible and near-infrared spectra confirm that 18493 is different from other Aneas family members. This spectral diversity might indicate that 18493 is an interloper or that it comes from the interior of the parent body.
- 15094 and 13463 in Makhaon family have a spectral behavior flatter than the other family members. Considering also that they do not dynamically belong to the Makhaon family for a cutoff value of 100 m/s, they can be considered as interlopers.
- No relation has been found between color indices and dynamical characteristics. All the spectra have similar behaviors independently from proper elements. Considering the size, small objects have a slightly larger dispersion in the spectral slope than the large ones. This feature could be possibly due to different degrees of space weathering ageing.

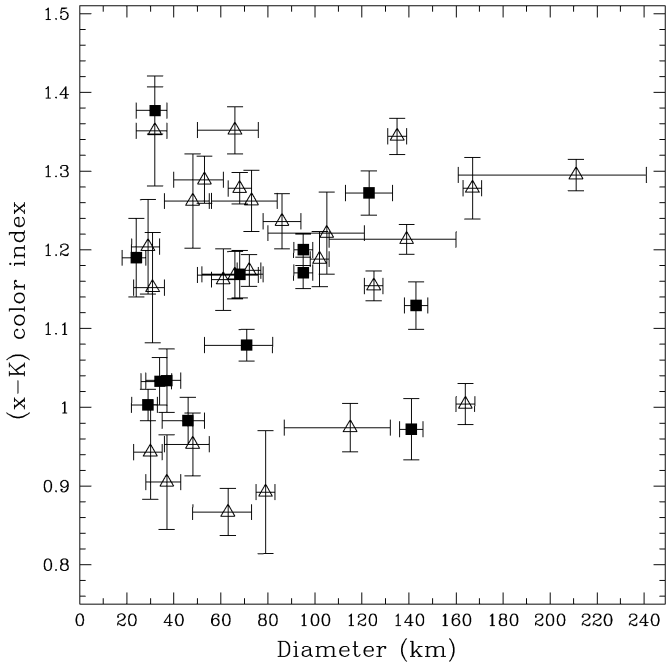

Fig. 8. The x–K color index (derived from the difference between the reflectance at 0.85 and at 2.2 μm), vs the estimated diameter. The (x–K) color index includes the solar color both for our and Emery and Brown (2004) data. Open triangles correspond to data on the L4 cloud, while black squares are for the L5 cloud.

On the basis of these results we can suppose that the parent bodies of all the analyzed families had a quite homogeneous structure. Also the whole population of Jupiter Trojans is quite homogeneous, even considering the two L4 and L5 clouds. Small members show a wide range of variation of their spectral slopes probably as a consequence of the different level of ageing due to space weathering of fragments coming from the interior or the surface of the parent bodies. Larger members show a smaller range of variation of their spectral slope. Their spectra have redder behavior which is probably a consequence of the ageing effect produced by space weathering processes

on the surface of the parent body. Icy component, if present, is not detected. Laboratory experiments are still needed to investigate the mechanism able to hide the ices which should be present of the surface of objects formed at large heliocentric distances.

Acknowledgments

We thank C. Beaugé and F. Roig for kindly providing us with updated Trojan family list. We thank D. Lazzaro and R.P. Binzel for having revised this paper, providing useful comments. E. Dotto, invited scientist at the European Southern Observatory on February–March 2003, thanks all the ESO staff for the hospitality.

Appendix A

Table A.1
Observational circumstances for visible spectroscopy of L4 family Trojans—ESO-NTT EMMI

Object	Night	UT start (hh:mm)	Slit ($''$)	Airm.	T_{exp} (s)	Solar analog (airmass)
12917	10 Apr. 03	01:27	1	1.29	1200	SA102-1081 (1.40)
12917	10 Apr. 03	04:36	1	1.11	900	SA107-684 (1.15)
13463	11 Apr. 03	00:59	1	1.55	1200	SA107-684 (1.49)
13463	11 Apr. 03	02:28	1	1.14	1200	SA107-684 (1.16)
15094	11 Apr. 03	07:19	1	1.18	900	SA107-684 (1.16)
15535	10 Apr. 03	08:08	1	1.45	900	SA102-1081 (1.40)
15535	10 Apr. 03	08:44	1	1.69	900	SA107-684 (1.54)
20738	10 Apr. 03	05:35	1	1.34	1200	SA102-1081 (1.40)
20738	10 Apr. 03	06:09	1	1.48	1200	SA102-1081 (1.40)
24390	11 Apr. 03	04:05	1	1.24	1200	SA107-684 (1.16)

Table A.2
Observational circumstances for visible spectroscopy of L4 family Trojans—TNG DOLORES

Object	Night	UT start (hh:mm)	Slit ($''$)	Airm.	T_{exp} (s)	Solar analog (airmass)
1647	06 May 03	22:49	2	1.2	600	SA P330E (1.2)
1647	06 May 03	22:59	2	1.2	600	SA P330E (1.2)
4035	07 May 03	01:16	2	1.6	600	SA P330E (1.2)
4035	07 May 03	01:27	2	1.6	600	SA P330E (1.2)
5244	07 May 03	00:03	2	1.3	600	SA P330E (1.2)
5244	07 May 03	00:13	2	1.3	600	SA P330E (1.2)
5258	06 May 03	22:09	2	1.2	600	SA P330E (1.2)
5258	06 May 03	22:19	2	1.2	600	SA P330E (1.2)
6545	07 May 03	00:38	2	1.7	600	SA P330E (1.2)
6545	07 May 03	00:48	2	1.7	600	SA P330E (1.2)
11351	07 May 03	02:53	2	1.8	600	SA P330E (1.2)
12921	07 May 03	01:59	2	1.3	600	SA P330E (1.2)
12921	07 May 03	02:09	2	1.3	600	SA P330E (1.2)
20738	06 May 03	23:26	2	1.1	600	SA P330E (1.2)
20738	06 May 03	23:36	2	1.1	600	SA P330E (1.2)

Table A.3
Observational circumstances for photometric data of L5 family Trojans—ESO-VLT ISAAC

Object	Night	UT start (hh:mm)	Filter	Airm.	T_{exp} (s × n_{acq})
1172	11 Nov. 02	07:57	J	1.475	1.7 × 2
1172	11 Nov. 02	08:02	H	1.488	1.7 × 2
1172	11 Nov. 02	08:07	K	1.501	1.7 × 2
1871	09 Nov. 02	01:01	J	1.757	30 × 4
1871	09 Nov. 02	02:44	J	1.247	60 × 4
1871	10 Nov. 02	01:17	J	1.594	60 × 5
1871	09 Nov. 02	01:06	H	1.710	15 × 4
1871	09 Nov. 02	02:44	H	1.236	60 × 4
1871	10 Nov. 02	01:03	H	1.694	15 × 4
1871	09 Nov. 02	01:12	K	1.664	15 × 4
1871	09 Nov. 02	02:44	K	1.213	30 × 2
1871	10 Nov. 02	01:09	K	1.650	15 × 4
15502	10 Nov. 02	02:20	J	1.963	30 × 4
15502	10 Nov. 02	04:15	J	1.986	30 × 4
15502	10 Nov. 02	02:25	H	1.948	15 × 4
15502	10 Nov. 02	04:03	H	1.949	10 × 4
15502	10 Nov. 02	02:31	K	1.934	15 × 4
15502	10 Nov. 02	04:09	K	1.967	10 × 4
18493	09 Nov. 02	07:33	J	1.287	60 × 4
18493	10 Nov. 02	07:27	J	1.283	60 × 4
18493	09 Nov. 02	07:38	H	1.297	20 × 4
18493	10 Nov. 02	07:32	H	1.292	10 × 4
18493	09 Nov. 02	07:44	K	1.308	20 × 4
18493	10 Nov. 02	07:38	K	1.305	10 × 4
23694	10 Nov. 02	04:37	J	1.217	30 × 4
23694	10 Nov. 02	04:43	H	1.219	10 × 4
23694	10 Nov. 02	04:49	K	1.221	10 × 4
30698	09 Nov. 02	03:40	J	1.443	60 × 4
30698	11 Nov. 02	03:28	J	1.451	15 × 4
30698	09 Nov. 02	03:46	H	1.426	30 × 4
30698	11 Nov. 02	03:34	H	1.434	5 × 4
30698	09 Nov. 02	03:53	K	1.409	20 × 4
30698	11 Nov. 02	03:40	K	1.416	3 × 6

Table A.4
Observational circumstances for photometric data of L4 family Trojans—ESO-VLT ISAAC

Object	Night	UT start (hh:mm)	Filter	Airm.	T_{exp} (s × n_{acq})
12917	10 Apr. 03	00:20	J	1.68	15 × 4
12917	10 Apr. 03	00:27	H	1.63	5 × 4
12917	10 Apr. 03	00:34	K	1.58	3 × 4
13463	11 Apr. 03	00:20	J	1.93	15 × 4
13463	11 Apr. 03	00:20	H	1.93	5 × 4
13463	11 Apr. 03	00:33	K	1.78	3 × 4
15094	11 Apr. 03	06:00	J	1.04	15 × 4
15094	11 Apr. 03	06:06	H	1.05	5 × 4
15094	11 Apr. 03	06:13	K	1.05	3 × 4
15535	10 Apr. 03	07:50	J	1.30	15 × 4
15535	10 Apr. 03	07:56	H	1.32	5 × 4
15535	10 Apr. 03	08:03	K	1.35	3 × 4
20738	10 Apr. 03	04:43	J	1.16	15 × 4
20738	10 Apr. 03	04:49	H	1.17	5 × 4
20738	10 Apr. 03	04:56	K	1.18	3 × 4
24390	11 Apr. 03	03:05	J	1.35	15 × 4
24390	11 Apr. 03	03:11	H	1.33	5 × 4
24390	11 Apr. 03	03:18	K	1.30	3 × 4

Table A.5
Observational circumstances for near-infrared spectroscopy of L5 and L4 family Trojans—ESO-VLT ISAAC

Object	Night	UT start (hh:mm)	Filter	Airm.	T_{exp} (s × n_{acq})	Slit ($''$)	Solar analog (airmass)
L5							
1172	11 Nov. 02	08:18	J	1.53	30 × 14	1.0	La93-101 (1.16)
1172	11 Nov. 02	08:39	H	1.61	30 × 4	1.0	La93-101 (1.17)
1172	11 Nov. 02	08:45	K	1.64	30 × 8	1.0	HD209847 (1.77)
1871	09 Nov. 02	01:30	J	1.53	60 × 8	1.0	La93-101 (1.50)
1871	10 Nov. 02	01:31	J	1.50	120 × 12	1.0	La93-101 (1.55)
1871	09 Nov. 02	01:48	H	1.44	120 × 8	1.0	HD209847 (1.03)
1871	09 Nov. 02	02:15	K	1.32	180 × 8	1.0	La93-101 (1.44)
15502	10 Nov. 02	02:45	J	1.90	60 × 10	1.0	HD209847 (2.10)
15502	10 Nov. 02	03:10	H	1.88	60 × 12	1.0	HD209847 (2.10)
15502	10 Nov. 02	03:27	K	1.88	60 × 14	1.0	HD209847 (2.12)
18493	10 Nov. 02	08:31	J	1.48	120 × 12	1.0	HD209847 (1.26)
18493	10 Nov. 02	07:52	H	1.34	180 × 10	1.0	La98-978 (1.13)
18493	09 Nov. 02	07:56	K	1.34	120 × 30	1.0	La98-978 (1.15)
23694	10 Nov. 02	05:00	J	1.23	60 × 10	1.0	HD209847 (1.26)
23694	10 Nov. 02	05:22	H	1.25	180 × 8	1.0	HD209847 (1.28)
23694	10 Nov. 02	05:55	K	1.32	180 × 12	1.0	HD209847 (1.29)
30698	09 Nov. 02	04:11	J	1.37	60 × 18	1.0	La93-101 (1.50)
30698	09 Nov. 02	04:50	H	1.33	120 × 16	1.0	La93-101 (1.47)
30698	09 Nov. 02	05:33	H	1.34	120 × 32	1.0	La93-101 (1.15)
L4							
12917	10 Apr. 03	00:53	J	1.44	180 × 4	1.0	La102-1081 (1.40)
12917	10 Apr. 03	01:17	H	1.32	180 × 16	1.0	La102-1081 (1.39)
12917	10 Apr. 03	02:27	K	1.12	180 × 28	1.5	La102-1081 (1.24)
13463	11 Apr. 03	00:49	J	1.63	120 × 4	1.0	La102-1081 (1.77)
13463	11 Apr. 03	02:05	H	1.22	180 × 6	1.0	La98-978 (1.17)
13463	11 Apr. 03	01:16	K	1.43	180 × 12	1.0	La102-1081 (1.35)
15094	11 Apr. 03	09:11	J	1.64	180 × 6	1.0	La102-1081 (1.77)
15094	11 Apr. 03	08:09	H	1.28	180 × 16	1.0	La102-1081 (1.36)
15094	11 Apr. 03	06:28	K	1.06	180 × 28	1.0	La102-1081 (1.10)
15535	10 Apr. 03	08:20	J	1.43	60 × 6	1.5	La107-998 (1.46)
15535	10 Apr. 03	08:30	H	1.48	60 × 8	1.5	La107-998 (1.48)
15535	10 Apr. 03	08:43	K	1.57	60 × 12	1.5	La107-998 (1.57)
20738	10 Apr. 03	05:14	H	1.21	180 × 8	1.5	La102-1081 (1.23)
20738	10 Apr. 03	05:58	K	1.33	180 × 18	1.5	La102-1081 (1.24)
24390	11 Apr. 03	05:15	J	1.13	120 × 4	1.0	La102-1081 (1.10)
24390	11 Apr. 03	03:34	H	1.25	180 × 8	1.0	La102-1081 (1.10)
24390	11 Apr. 03	04:08	K	1.18	180 × 18	1.0	La102-1081 (1.10)

Table A.6
Observational circumstances for near-infrared spectroscopy of L5 family Trojans—TNG NICS + Amici

Object	Night	UT start (hh:mm)	Airm.	T_{exp} (s × n_{acq})	Slit ($''$)	Solar analog (airmass)
L5						
2223	30 Nov. 02	04:36	1.4–1.6	120 × 8	1.5	1,2,4,5
2223	01 Dec. 02	04:47	1.5–1.7	60 × 24	1.5	1,2,5
2357	01 Dec. 02	04:47	1.5–1.7	60 × 4	1.5	1,2,4,5
2357	02 Dec. 02	05:10	1.9–2.4	60 × 28	1.5	1,2,3,4
5130	30 Nov. 02	20:09	1.2	60 × 16	1.5	1,2,5
6998	30 Nov. 02	20:09	1.2	60 × 72	1.5	1,2,5
18940	30 Nov. 02	00:46	1.0–1.1	120 × 12	1.5	1,2,4,5
18940	30 Nov. 02	21:28	1.2	120 × 4	1.5	1,2,5

Solar analog and airmasses (30 Nov.; 1 Dec.; 2 Dec.): 1—HD209847 (2.15; 1.42; 1.43); 2—Hy 142 (1.13; 1.04 and 2.11; 1.07 and 2.38); 3—Landolt 112-1133 (–; –; 1.43); 4—Landolt 98-978 (1.38; –; 1.23 and 1.43); 5—Landolt 93-101 (1.14 and 1.23; 1.76; –).

Table A.7
Observational circumstances for near-infrared spectroscopy of L4 family Trojans—TNG NICS + Amici

Object	Night	UT start (hh:mm)	Airm.	T_{exp} (s × n_{acq})	Slit ($''$)	Solar analog (airmass)
L4						
1647	05 May 03	22:44	1.2	90 × 6	1.5	1,2,3
5258	05 May 03	23:11	1.3	90 × 6	1.5	1,2,3
5244	06 May 03	00:39	1.4	90 × 6	1.5	1,2,3
6545	03 May 03	23:30	1.6	90 × 6	1.5	1,2,3
4035	03 May 03	23:05	1.4	90 × 6	1.5	1,2,3
11351	04 May 03	01:33	1.6	90 × 12	1.5	1,2,3
12921	04 May 03	00:16	1.1	90 × 24	1.5	1,2,3

Solar analog and airmasses (03 May; 05 May): 1—Land102-10 (1.19; 1.16); 2—Land107-68 (1.2–1.7; 1.16); 3—Land110-36 (1.14; 1.14).

References

Barucci, M.A., Boehnhardt, H., Dotto, E., Doressoundiram, A., Romon, J., Lazzarin, M., Fornasier, S., de Bergh, C., Tozzi, G.P., Delsanti, A., Hainaut, O., Barrera, L., Birkle, K., Meech, K., Ortiz, J.L., Sekiguchi, T., Thomas, N., Watanabe, J., West, R.M., Davies, J.K., 2002. Visible and near-infrared spectroscopy of the Centaur 32532 (2001 PT13). ESO large program on TNOs and centaurs: First spectroscopy results. Astron. Astrophys. 392, 335–339.

Beaugé, C., Roig, F., 2001. A semianalytical model for the motion of the Trojan asteroids: Proper elements and families. Icarus 53, 391–415.

Bendjoya, P., Cellino, A., Di Martino, M., Saba, L., 2004. Spectroscopic observations of Jupiter Trojans. Icarus 168, 374–384.

Bowell, E., Hapke, B., Domingue, D., Lumme, K., Peltoniemi, J., Harris, A.W., 1989. Application of photometric models to asteroids. In: Binzel, R.P., Gehrels, T., Matthews, M.S. (Eds.), Asteroids II. Univ. of Arizona Press, Tucson, pp. 524–556.

Clark, R.N., Swayze, G.A., Gallagher, A.J., King, T.V.V., Calvin, W.M., 1993. U.S. Geological Survey Open File Report 93-592, http://speclab.cr.usgs.gov.

Cruikshank, D.P., Dalle Ore, C.M., Roush, T.L., Geballe, T.R., Owen, T.C., de Bergh, C., Cash, M.D., Hartmann, W.K., 2001. Constraints on the composition of Trojan Asteroid 624 Hektor. Icarus 153, 348–360.

Cruikshank, D.P., Dalle Ore, C.M., 2003. Spectral models of Kuiper belt objects and centaurs. Earth Moon Planets 92, 315–330.

de Bergh, C., Boehnhardt, H., Barucci, M.A., Lazzarin, M., Fornasier, S., Romon-Martin, J., Tozzi, G.P., Doressoundiram, A., Dotto, E., 2004. Aqueous altered silicates at the surface of two Plutinos? Astron. Astrophys. 416, 791–798.

Dotto, E., Barucci, M.A., Leyrat, C., Romon, J., de Bergh, C., Licandro, J., 2003a. Unveiling the nature of 10199 Chariklo: Near-infrared observations and modeling. Icarus 164, 122–126.

Dotto, E., Barucci, M.A., de Bergh, C., 2003b. Colors and composition of the centaurs. Earth Moon Planets 92, 157–167.

Dotto, E., Barucci, M.A., Boehnhardt, H., Romon, J., Doressoundiram, A., Peixinho, N., de Bergh, C., Lazzarin, M., 2003c. Searching for water ice on 47171 1999 TC36, 1998 SG35, and 2000 QC243: ESO large program on TNOs and centaurs. Icarus 162, 408–414.

Dumas, C., Owen, T., Barucci, M.A., 1998. Near-infrared spectroscopy of low-albedo surfaces of the Solar System: Search for the spectral signature of dark material. Icarus 133, 221–232.

Emery, J.P., Brown, R.H., 2001. Near-infrared spectroscopy of Trojan asteroids: Implications for the evolution of the Solar System. Lunar Planet. Sci. 32. Abstract 1385.

Emery, J.P., Brown, R.H., 2003. Constraints on the surface composition of Trojan asteroids from near-infrared (0.8–4.0 μm) spectroscopy. Icarus 164, 104–121.

Emery, J.P., Brown, R.H., 2004. The surface composition of Trojan asteroids: Constraints set by scattering theory. Icarus 170, 131–152.

Fernandez, Y.R., Sheppard, S.S., Jewitt, D.C., 2003. The albedo distribution of jovian Trojan asteroids. Astron. J. 126, 1563–1574.

Fitzsimmons, A., Dahlgren, M., Lagerkvist, C.I., Magnusson, P., Williams, I.P., 1994. A spectroscopic survey of D-type asteroids. Astron. Astrophys. 282, 634–642.

Fornasier, S., Dotto, E., Marzari, F., Barucci, M.A., Boehnhardt, H., Hainaut, O., de Bergh, C., 2004a. Visible spectroscopic and photometric survey of L5 Trojans: Investigation of dynamical families. Icarus 172, 221–232.

Fornasier, S., Dotto, E., Barucci, M.A., Barbieri, C., 2004b. Water ice on the surface of the large TNO 2004 DW. Astron. Astrophys. 422, L43–L46.

Hudson, R.L., Moore, M.H., 1999. Laboratory studies of the formation of methanol and other organic molecules by water + carbon monoxide radiolysis: Relevance to comets, icy satellites, and interstellar ices. Icarus 140, 451–461.

Hunt, L.K., Mannucci, F., Testi, L., Migliorini, S., Stanga, R.M., Baffa, C., Lisi, F., Vanzi, L., 1998. Northern JHK standard stars for array detectors. Astron. J. 115, 2594–2603.

Jewitt, D.C., Luu, J.X., 1990. CCD spectra of asteroids. II. The Trojans as spectral analogs of cometary nuclei. Astron. J. 100, 933–944.

Jewitt, D.C., Trujillo, C.A., Luu, J.X., 2000. Population and size distribution of small jovian Trojan asteroids. Astron. J. 120, 1140–1147.

Jones, T.D., Lebofsky, L.A., Lewis, J.S., Marley, M.S., 1990. The composition and origin of the C, P, and D asteroids—Water as a tracer of thermal evolution in the outer belt. Icarus 88, 172–192.

Khare, B.N., Sagan, C., Arakawa, E.T., Suits, F., Callcott, T.A., Williams, M.W., 1984. Optical constants of organic tholins produced in a simulated titanian atmosphere—From soft X-ray to microwave frequencies. Icarus 60, 127–137.

Khare, B.N., Thompson, W.R., Sagan, C., Arakawa, E.T., Meisse, C., Gilmour, I., 1991. Optical constants of kerogen from 0.15 to 40 micron: Comparison with meteoritic organics. In: Levasseur-Regours, A.C., Hasegawa, H. (Eds.), Origin and Evolution of Interplanetary Dust, IAU Colloq. 126. Kluwer Academic, Dordrecht. ASSL 173, 99.

Khare, B.N., Thompson, W.R., Cheng, L., Chyba, C., Sagan, C., Arakawa, E.T., Meisse, C., Tuminello, P.S., 1993. Production and optical constraints of ice tholin from charged particle irradiation of (1:6) C_2H_6/H_2O at 77 K. Icarus 103, 290–300.

Landolt, A.U., 1992. UBVRI photometric standard stars in the magnitude range 11.5–16.0 around the celestial equator. Astron. J. 104, 340–371, 436–491.

Lazzarin, M., Barbieri, C., Barucci, M.A., 1995. Visible spectroscopy of dark, primitive asteroids. Astron. J. 110, 3058–3072.

Licandro, J., Ghinassi, F., Testi, L., 2002. Infrared spectroscopy of the largest known trans-neptunian object 2001 KX75. Astron. Astrophys. 388, L9–L12.

Luu, J.X., Jewitt, D., Cloutis, E., 1994. Near-infrared spectroscopy of primitive Solar System objects. Icarus 109, 133–144.

Marzari, F., Scholl, H., Murray, C., Lagerkvist, C., 2003. Origin and evolution of Trojan asteroids. In: Bottke, W., Cellino, A., Paolicchi, P., Binzel, R.P. (Eds.), Asteroids III. Univ. of Arizona Press, Tucson, pp. 725–738.

McDonald, G.D., Thompson, W.R., Heinrich, M., Khare, B.N., Sagan, C., 1994. Chemical investigation of Titan and Triton tholins. Icarus 108, 137–145.

McDonald, G.D., Whited, L.J., Deruiter, C., Khare, B.N., Patnaik, A., Sagan, C., 1996. Production and chemical analysis of cometary ice tholins. Icarus 122, 107–117.

Moore, M.H., Donn, B., Khanna, R., A'Hearn, M.F., 1983. Studies of proton-irradiated cometary-type ice mixtures. Icarus 54, 388–405.

Morbidelli, A., Levinson, H.F., Tsiganis, K., Gomes, R., 2005. Chaotic capture of Jupiter's Trojan asteroids in the early Solar System. Nature 435, 462–464.

Moroz, L.V., Arnold, G., Korochantsev, A.V., Wasch, R., 1998. Natural solid bitumens as possible analogs for cometary and asteroid organics. Icarus 134, 253–268.

Persson, S.E., Murphy, D.C., Krzeminski, W., Roth, M., Rieke, M.J., 1998. A new system of faint near-infrared standard stars. Astron. J. 116, 2475–2488.

Romon, J., de Bergh, C., Barucci, M.A., Doressoundiram, A., Cuby, J.-G., Le Bras, A., Douté, S., Schmitt, B., 2001. Photometric and spectroscopic observations of Sycorax, satellite of Uranus. Astron. Astrophys. 376, 310–315.

Strazzulla, G., 1998. Chemistry of ice induced by bombardment with energetic charged particles. In: Schmitt, B., de Bergh, C., Festou, M. (Eds.), Solar System Ices. Kluwer Academic, Dordrecht. ASSL 281.

Tancredi, G., Fernandez, J.A., Rickman, H., Licandro, J., 2006. Nuclear magnitudes and size distribution of Jupiter family comets. Icarus. In press.

Thompson, W.R., Murray, B.G.J.P.T., Khare, B.N., Sagan, C., 1987. Coloration and darkening of methane clathrate and other ices by charged particle irradiation—Applications to the outer Solar System. J. Geophys. Res. 92, 14933–14947.

Zubko, V.G., Mennella, V., Colangeli, L., Bussoletti, E., 1996. Optical constants of cosmic carbon analogue grains. I. Simulation of clustering by a modified continuous distribution of ellipsoids. Mon. Not. R. Astron. Soc. 282, 1321–1329.